

# Nanowires and sidewall Bragg gratings in silicon as enabling technologies for microwave photonic filters

Lawrence R. Chen,<sup>1,\*</sup> Jia Li,<sup>1,2</sup> Mina Spasojevic,<sup>1</sup> and Rhys Adams<sup>1,3</sup>

<sup>1</sup>Department of Electrical and Computer Engineering, McGill University, Montreal, QC H3A 0E9 Canada

<sup>2</sup>Ciena, Ottawa, ON K2H 8E9 Canada

<sup>3</sup>Department of Physics, CEGEP Vanier College, Montreal, QC H4L 3X9 Canada

\*[lawrence.chen@mcgill.ca](mailto:lawrence.chen@mcgill.ca)

**Abstract:** We describe the use of various silicon photonic device technologies to implement microwave photonic filters (MPFs). We demonstrate four-wave mixing in a silicon nanowire waveguide (SNW) to increase the number of taps for MPFs based on finite impulse response filter designs. Using a 12 mm long SNW reduces the footprint by five orders of magnitude compared to silica highly nonlinear fiber while only requiring approximately two times more input power. We also demonstrate optical delays based on serial sidewall Bragg grating arrays and step-chirped sidewall Bragg gratings in silicon waveguides. We obtain up to 63 ps delay in discrete steps from 15 ps to 32 ps over a wide bandwidth range from 33 nm to at least 62 nm. These components can be integrated with other silicon-based components such as integrated spectral shapers and modulators to realize a fully integrated MPF.

©2013 Optical Society of America

OCIS codes: (130.3120) Integrated optics devices; (060.5625) Radio frequency photonics.

---

## References and links

1. J. Capmany and D. Novak, "Microwave photonics combines two worlds," *Nat. Photonics* **1**(6), 319–330 (2007).
2. J. P. Yao, "Microwave photonics," *J. Lightwave Technol.* **27**(3), 314–335 (2009).
3. J. Capmany, J. Mora, I. Gasulla, J. Sancho, J. Lloret, and S. Sales, "Microwave photonic signal processing," *J. Lightwave Technol.* **31**(4), 571–586 (2013).
4. J. Capmany, B. Ortega, and D. Pastor, "A tutorial on microwave photonic filters," *J. Lightwave Technol.* **24**(1), 201–229 (2006).
5. J. Capmany, J. Mora, B. Ortega, and D. Pastor, "High-quality low-cost online-reconfigurable microwave photonic transversal filter with positive and negative coefficients," *IEEE Photon. Technol. Lett.* **17**(12), 2730–2732 (2005).
6. J. H. Lee, Y. M. Chang, Y.-G. Han, H. Chung, and S. B. Lee, "Flexibility tunable microwave photonics FIR filter incorporating wavelength spacing programmable, arrayed micro-mirror based optical filter," *Electron. Lett.* **42**(14), 812–814 (2006).
7. X. Yi, T. X. H. Huang, and R. A. Minasian, "Tunable and reconfigurable photonic signal processor with programmable all-optical complex coefficients," *IEEE Trans. Microw. Theory Tech.* **58**(11), 3088–3093 (2010).
8. E. Hamidi, D. E. Leaird, and A. M. Weiner, "Tunable programmable microwave photonic filters based on an optical frequency comb," *IEEE Trans. Microw. Theory Tech.* **58**(11), 3269–3278 (2010).
9. D. Marpaung, C. Roeloffzen, R. Heideman, A. Leinse, S. Sales, and J. Capmany, "Integrated microwave photonics," *Lasers & Photon. Rev.* doi: 10.1002/lpor.201200032. (2013).
10. H.-W. Chen, A. W. Fang, J. D. Peters, Z. Wang, J. Bovington, D. Liang, and J. E. Bowers, "Integrated microwave photonic filter on a hybrid silicon platform," *IEEE Trans. Microw. Theory Tech.* **58**(11), 3213–3219 (2010).
11. E. J. Norberg, R. S. Guzzon, J. S. Parker, L. A. Johansson, and L. A. Coldren, "Programmable photonic microwave filters monolithically integrated in InP/InGaAsP," *J. Lightwave Technol.* **29**(11), 1611–1619 (2011).
12. A. Byrnes, R. Pant, E. Li, D.-Y. Choi, C. G. Poulton, S. Fan, S. Madden, B. Luther-Davies, and B. J. Eggleton, "Photonic chip based tunable and reconfigurable narrowband microwave photonic filter using stimulated Brillouin scattering," *Opt. Express* **20**(17), 18836–18845 (2012).
13. J. Leuthold, C. Koos, and W. Freude, "Nonlinear silicon photonics," *Nat. Photonics* **4**(8), 535–544 (2010).

14. B. Vidal, J. Palací, and J. Capmany, "Reconfigurable photonic microwave filter based on four-wave mixing," *IEEE Photon. J.* **4**(3), 759–764 (2012).
15. J. Li, R. Adams, Z. Saraç, D. Berardo, and L. R. Chen, "A reconfigurable microwave photonic filter based on four wave mixing in a silicon nanophotonic waveguide," presented at Photonics North, Ottawa, ON, Canada, 3–5 June 2013.
16. A. C. Turner, C. Manolatu, B. S. Schmidt, M. Lipson, M. A. Foster, J. E. Sharping, and A. L. Gaeta, "Tailored anomalous group-velocity dispersion in silicon channel waveguides," *Opt. Express* **14**(10), 4357–4362 (2006).
17. M. H. Khan, H. Sehn, Y. Xuan, L. Zhao, S. Xiao, D. E. Leaird, A. M. Weiner, and M. Qi, "Ultrabroad-bandwidth arbitrary radiofrequency waveform generation with a silicon photonic chip-based spectral shaper," *Nat. Photonics* **4**(2), 117–122 (2010).
18. F. Morichetti, A. Melloni, C. Ferrari, and M. Martinelli, "Error-free continuously-tunable delay at 10 Gbit/s in a reconfigurable on-chip delay-line," *Opt. Express* **16**(12), 8395–8405 (2008).
19. A. Melloni, A. Canciamilla, C. Ferrari, F. Morichetti, L. O'Faolain, T. F. Krauss, R. M. De La Rue, A. Samarelli, and M. Sorel, "Tunable delay lines in Silicon photonics: coupler resonators and photonic crystals, a comparison," *IEEE Photon. J.* **2**(2), 181–194 (2010).
20. D. T. H. Tan, K. Ikeda, R. E. Saperstein, B. Slutsky, and Y. Fainman, "Chip-scale dispersion engineering using chirped vertical gratings," *Opt. Lett.* **33**(24), 3013–3015 (2008).
21. D. T. H. Tan, K. Ikeda, and Y. Fainman, "Coupled chirped vertical gratings for on chip group velocity dispersion engineering," *Appl. Phys. Lett.* **95**(14), 141109 (2009).
22. I. Giunttoni, D. Stolarek, D. I. Kroushkov, J. Bruns, L. Zimmermann, B. Tillack, and K. Petermann, "Continuously tunable delay line based on SOI tapered Bragg gratings," *Opt. Express* **20**(10), 11241–11246 (2012).
23. E. Mortazy, B. Le Drogoff, J. Azaña, M. Chaker, and A. Tehranchi, "Chirped Bragg grating in silicon based rib waveguide," in *Proc. 7th Workshop on Fiber and Optical Passive Components*, Montreal, Canada, July 2011, pp. 1–4.
24. S. Khan and S. Fathpour, "Complementary apodized grating waveguides for tunable optical delay lines," *Opt. Express* **20**(18), 19859–19867 (2012).
25. M. Spasojevic and L. R. Chen, "Tunable optical delay line in SOI implemented with step chirped Bragg gratings serial grating arrays," presented at Photonics North, Ottawa, ON, Canada, 3–5 June 2013.
26. M. Lipson, "Silicon photonics: the optical spice rack," *Electron. Lett.* **45**(12), 576–577 (2009).
27. Q. Wang, H. Rideout, F. Zeng, and J. P. Yao, "Millimeter-wave frequency tripling based on four-wave mixing in a semiconductor optical amplifier," *IEEE Photon. Technol. Lett.* **18**(23), 2460–2462 (2006).
28. L. Xu, C. Li, S. M. G. Lo, and H. K. Tsang, "Millimeter wave generation using four wave mixing in silicon waveguidem" in *Proc. Opto-Electon. and Comm. Conference*, Sapporo, Japan, July 2010, pp. 860–861.

## 1. Introduction

There is considerable interest in exploiting photonic approaches and technologies for generating, transmitting, detecting, and processing microwave and millimeter wave signals as an alternative to conventional electronic approaches [1–3]. The advantages of using photonic components include low loss, compactness, and immunity to electromagnetic interference. A microwave photonic filter (MPF) is an essential building block of microwave photonic signal processing and provides many functionalities, e.g., in communications systems where filtering high-speed signals is essential to ensure conformity to regulations, to enhance immunity to channel fading and noise, or for application in opto-electronic oscillators, radio-over-fiber systems, microwave radar, and photonic beamsteering of phased-arrayed antennas. The design of MPFs with reconfiguration and/or tuning capabilities has been the subject of intense research and many structures have been proposed and important results have been demonstrated [4–8].

MPF filters employ typically discrete components resulting in bulky, benchtop implementations. To address issues related to compactness, stability, power consumption, and ultimately mass production for cost, the development of integrated (single chip) MPFs is of great importance. Indeed, several integrated MPFs and MPF subsystems have been reported [3,9–12]; those based in silicon are especially attractive for their compatibility with CMOS processing [13].

In this paper, we describe the implementation of two important MPF building blocks using silicon photonic technologies. First, in Section 2, we show the use of four wave mixing (FWM) in silicon nanowire waveguides (SNWs) to increase the number of taps for MPFs based on finite impulse response (FIR) filter designs and discuss possibilities to achieve reconfigurability. Second, in Section 3, we demonstrate the implementation of optical delays

using sidewall gratings in silicon waveguides. Finally, we describe how the various building blocks can potentially be integrated.

## 2. Silicon nanowires

There are a number of approaches for implementing MPFs. One of the most straightforward is based on concepts from digital FIR filter design, whereby multiple delayed and weighted versions of the input signal are added together [4]. This incoherent approach is preferable since it is easy to configure and is stable against environmental perturbations. In this type of filter, the microwave signal is conveyed on different optical carriers (i.e., wavelengths) or taps through intensity modulation, e.g., via an electro-optic Mach-Zehnder modulator (MZM). The optical carriers are then delayed in time using delay lines or dispersive media before photodetection. To implement an  $n$ -tap MPF requires  $n$  laser sources. Recently, Vidal *et al.* demonstrated the use of FWM in a length of highly nonlinear fiber (HNLF) to increase the number of taps to control the MPF response [14]. In particular, by controlling the power levels of two pump waves, the number of idler signals generated (and hence the total number of taps) can be controlled. Moreover, the amplitude of each tap was adjusted using an optical filter based on a polarization controller and a short length of polarization maintaining fiber. Three, four, and five tap filter responses with uniform and apodized profiles were achieved.

In this section, we describe several developments that lend themselves to integration of the MPF demonstrated in [14]. First, we consider the use SNWs rather than HNLF for FWM. We control the tap levels in order to reconfigure the MPF response with a benchtop programmable filter [15]. This approach provides greater flexibility in terms of tap control compared to the optical filter used in [14]. We also compare results between using the SNWs and HNLF for FWM. Finally, we describe employing an integrated spectral shaper to replace the benchtop programmable filter.

### 2.1 Waveguide design

FWM is most efficient when the phase-matching condition is satisfied, which requires the pump wavelength to be located close to the zero dispersion wavelength in the anomalous group velocity dispersion (GVD) regime of the nonlinear medium (i.e.,  $\sim 1550$  nm for fiber optic communications). Since the material dispersion of silicon is large and normal, SNWs need to be designed carefully to tailor the waveguide dispersion such that anomalous GVD can be obtained [16].

We consider strip-based SNWs on silica with and without top oxide cladding layers. The SNWs consist of a thin silicon layer (thickness or height  $H = 220$  nm) deposited on a  $2\ \mu\text{m}$  thick oxide cladding. We then adjust the SNW width  $W$  (or effectively, the aspect ratio). Simulations show that anomalous dispersion can be realized at  $1550$  nm if  $440\ \text{nm} < W < 540$  nm for SNWs with a top oxide cladding. Moreover, the dispersion slope is nearly 0 around  $1550$  nm when  $W \approx 490$  nm, which is useful for broadband FWM. On the other hand, for SNWs without a top oxide cladding, anomalous dispersion can be obtained for  $W < 690$  nm; however, the waveguides cannot be too thin as the dispersion increases very rapidly.

Vertical grating couplers are used for input and output coupling and to ensure operation with TE-polarized light.

### 2.2 Waveguide characterization

We fabricated waveguides of different dimensions and lengths and used a pump-probe approach to characterize the FWM conversion efficiency. The pump and the probe are adjusted to be co-polarized. The pump wavelength is set at  $\lambda_{\text{pump}} = 1545$  nm with a power  $P_{\text{pump}} = 250$  mW while the probe wavelength is  $\lambda_{\text{probe}} = 1543$  nm with  $P_{\text{probe}} = 12$  mW. The FWM conversion efficiency  $\eta$  is defined as the power ratio between the generated idler and probe signal.

For SNWs 12 mm in length and without a top oxide cladding, the conversion efficiency is in the range  $-25.5 \text{ dB} < \eta < -23 \text{ dB}$  for  $630 \text{ nm} < W < 690 \text{ nm}$ ; on the other hand, with a top oxide cladding,  $-23 \text{ dB} < \eta < -22 \text{ dB}$  for  $490 \text{ nm} < W < 540 \text{ nm}$ . For the same pump power, the conversion efficiency is slightly higher for SNWs with a top oxide cladding; this is since the fiber-to-fiber insertion loss tends to be somewhat smaller,  $\sim 17 \text{ dB}$  compared to  $\sim 21 \text{ dB}$  (the loss from each vertical coupler is  $\sim 7.5 \text{ dB}$  and the propagation loss is  $1.5 \text{ dB/cm}$  compared to  $9.3 \text{ dB}$  and  $2.3 \text{ dB/cm}$  for SNWs without a top oxide cladding).

For SNWs with a top oxide cladding and  $W = 500 \text{ nm}$ , we characterized the dependence of  $\eta$  as a function of SNW length  $L$ . For  $P_{\text{pump}} = 250 \text{ mW}$ ,  $\eta$  increases from  $-28.6 \text{ dB}$  to  $-18.9 \text{ dB}$  as  $L$  is increased from  $4 \text{ mm}$  to  $28 \text{ mm}$ . The conversion efficiency does not increase linearly as a function of  $L$ , though, due to propagation loss.

Finally, we characterized the FWM conversion efficiency bandwidth using an SNW with a top oxide cladding with  $W = 500 \text{ nm}$  width and  $L = 12 \text{ mm}$ . The  $3 \text{ dB}$  bandwidth for FWM conversion efficiency is at least  $10 \text{ nm}$ ; the broad FWM bandwidth is attributed to the small anomalous dispersion and near-zero dispersion slope of the SNW design.

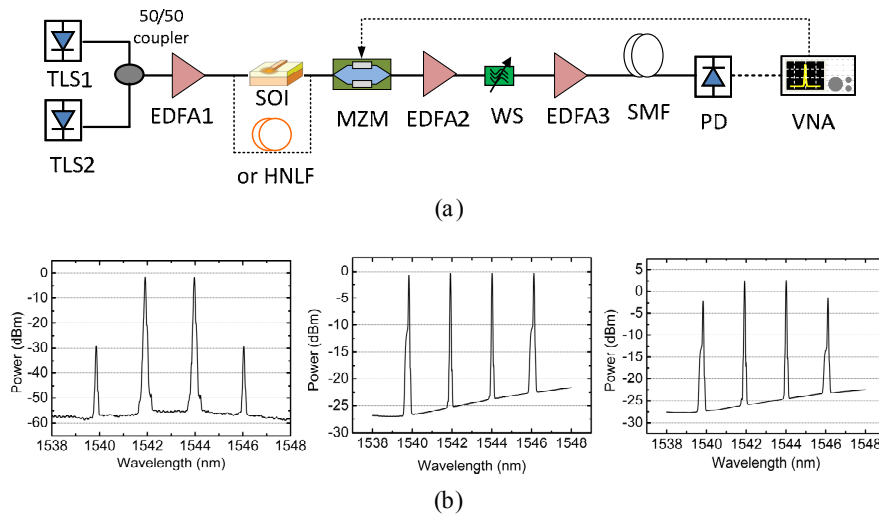


Fig. 1. (a) Experimental setup for 4-tap photonic microwave filter. (b) Optical spectra after FWM in the SNW (left), after the WS set to provide a uniform tap profile (center), and after the WS set to provide an apodized tap profile (right).

### 2.3 Experiment and results

We now demonstrate the use of SNWs for implementing an MPF. We use a  $12 \text{ mm}$  long SNW without a top oxide cladding with  $W = 650 \text{ nm}$ . The experimental setup is shown in Fig. 1(a). Two tunable continuous wave optical sources (set to  $1542 \text{ nm}$  and  $1544 \text{ nm}$ ) are amplified using a high-power erbium-doped fiber amplifier (EDFA) and coupled into the SNW. At least 2 idlers are generated via FWM in the SNW resulting in at least 4 taps. The optical carriers are modulated using a MZM and their amplitudes are controlled with a benchtop programmable optical filter (Finisar Waveshaper 1000-S, WS). We use  $4 \text{ km}$  of single mode fiber (SMF) as the dispersive medium giving rise to a time delay of  $\sim 136 \text{ ps}$  between taps; the corresponding free spectral range (FSR) of the MPF is  $\sim 7.4 \text{ GHz}$ . The MPF response is measured using a vector network analyzer (VNA). For comparison, we replace the SNW with  $1001 \text{ m}$  of silica HNLF having a zero dispersion wavelength of  $1556 \text{ nm}$ , a dispersion slope of  $0.02 \text{ ps}/(\text{nm}^2 \cdot \text{km})$ , and a nonlinear coefficient of  $10 \text{ W}^{-1} \cdot \text{km}^{-1}$ .

Figure 1(b) shows the output spectra from the SNW after amplification (i.e., after EDFA2) and before photodetection, i.e., with the WS set to provide a uniform or apodized profile.

Figure 2 compares the MPF responses obtained using the SNW or HNLf for the following cases: (a) 4 uniform taps, (b) 2 uniform taps but at twice the wavelength separation resulting in an MPF response with half the FSR of that in (a), (c) 3 uniform taps, and (d) 4 taps with an apodized profile. The simulated responses, based on the transfer function of an  $N$ -tap FIR filter, are also included. These results show that we can replace a length of HNLf with a 12 mm long SNW without compromising the quality of the MPF response. The power into the SNW after accounting for input coupling losses is about 13 dBm (note that this power level is similar to that used typically to realize all-optical signal processing functions such as FWM-based wavelength conversion of high-speed RZ-OOK data in SNWs [13]), whereas it is about 9 dBm when using HNLf. Hence, the current trade-off is that we reduce the length of the nonlinear medium by five orders of magnitude while increasing the input power level by approximately a factor of two.

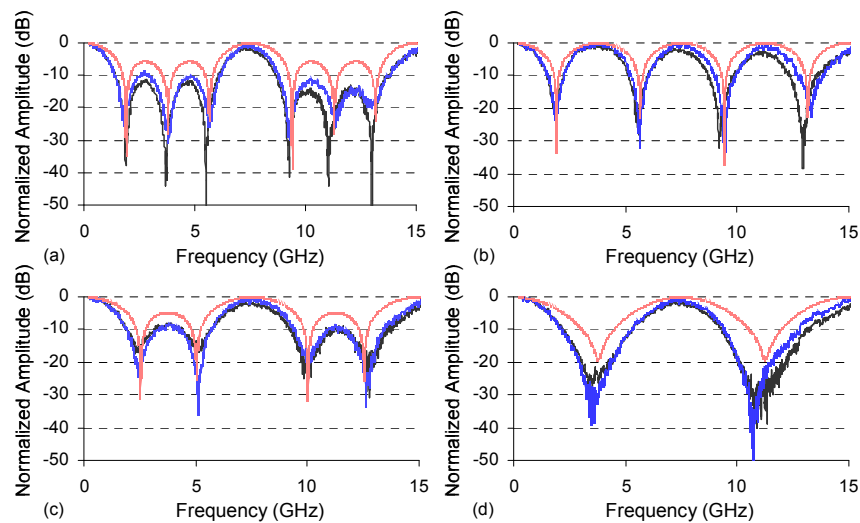


Fig. 2. Microwave photonic filter response for the following tap profiles: (a) [1,1,1,1]; (b) [1, 0, 1, 0]; (c) [1, 1, 1, 0]; and (d) [0.25, 1, 1, 0.25]. Experimental results using SNW (black) and HNLf (blue); simulations (red).

#### 2.4 Further integration

The results obtained above and in [14] demonstrate the potential for implementing a reconfigurable MPF. Although only a modest number of taps are used in both cases, it is possible to generate at least  $N$  taps starting from  $N/2$  sources. The use of a benchtop programmable optical filter also provides significant flexibility in controlling the tap weights; however, it does not lend itself readily to integration. To develop a more integrated solution, we can combine the use of SNWs with a programmable integrated spectral shaper. In particular, Khan *et al.* recently reported a silicon photonic chip-based spectral shaper for arbitrary waveform generation [17]. The integrated spectral shaper is based on cascaded microring resonators. Microheaters are placed above each ring to control independently the corresponding resonant wavelength. Moreover, by incorporating a Mach-Zehnder input coupler at the through port of each ring, further control over the depth of each resonance can be obtained. Thus, FWM generation in SNWs followed by the integrated spectral shaper will provide a straightforward means for increasing the number of taps as well as controlling their amplitudes. Note that this approach is more adapted to reconfiguring the shape of the MPF response as the wavelength spacing between optical carriers would largely be fixed. Tuning the MPF frequency requires either greater control over the wavelength spacing of the taps, or to change the delays between the taps.

### 3. Tunable optical delays

In Section 2, we described how FWM in SNWs can be used as one fundamental building block to generate the necessary taps when implementing MPFs based on FIR filter designs. A second fundamental building block is an optical delay. Optical delays are realized typically with either fiber delay lines (e.g., lengths of fiber) or grating-based structures such as linearly chirped fiber Bragg gratings (LCFBGs). For an MPF with a FSR of 10 GHz, a delay of 100 ps between taps is required; the wavelength spacing of the optical carriers used for the taps will then dictate the required dispersion of the delay medium to obtain the necessary delay. Fiber delay lines are attractive since they are generally broadband, i.e., can accommodate a large number of taps and/or tap spacings. However, long lengths of fiber are needed, e.g., several km's for a tap spacing of 100 GHz and a delay of 100 ps. On the other hand, LCFBGs can provide a dispersion of 100 ps/nm spanning several nanometers in significantly more compact forms. Tunable LCFBGs are also readily available [4].

Silicon-photonic-based delay lines have been realized using coupled ring resonators [18], photonic crystals [19], and various Bragg grating-based configurations including single or coupled chirped sidewall gratings [20,21] as well as tapered rib waveguide gratings [22]. By linearly chirping the period in sidewall gratings, relatively small delays (a few ps) over a bandwidth of tens of nm were demonstrated [20]; with tapered waveguides, significantly larger delays (up to 500 ps) were obtained, albeit over a narrower bandwidth (< 2 nm) [22]. The delays demonstrated to date may not be suitable for implementation in MPFs where large delays (e.g., tens to hundreds of ps) over large bandwidths (several to tens of nm) are required. Several designs have been proposed to meet these requirements, e.g., a step-chirped rib waveguide grating providing 50 ps delay over 15 nm [23] or complementary apodized sidewall gratings providing up to 275 ps over 3 nm [24]; however, they have not been realized experimentally.

In this section, we demonstrate discrete optical delay lines providing up to 65 ps delay in discrete steps from 15 ps to 32 ps over a wide bandwidth range from 35 nm to 70 nm (preliminary results are presented in [25]). The devices are fabricated on silicon-on-insulator using electron beam lithography and implemented through two different approaches: serial sidewall Bragg grating arrays and step-chirped sidewall Bragg gratings.

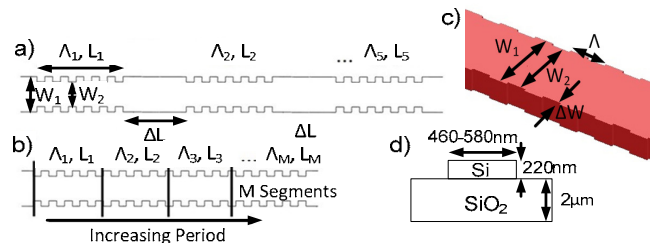


Fig. 3. Schematic diagram of silicon waveguide grating-based delays. (a) Serial grating arrays, (b) step-chirped gratings, (c) and (d) cross-sectional views.

#### 3.1 General design

Figure 3 shows a schematic of the two grating structures. The serial array [Fig. 3(a)] comprises a cascade of uniform gratings of different periods (each grating is characterized by a length  $L_i$  and period  $\Lambda_i$ ) physically separated by a constant length of waveguide ( $\Delta L$ ) that introduces a fixed delay for the different resonant wavelengths. When  $\Delta L \rightarrow 0$ , the serial array becomes a step-chirped grating [Fig. 3(b)].

Figure 3(c) shows a cross-sectional view of the sidewall gratings. The gratings were fabricated with shallow etch electron beam lithography on a 220 nm thick silicon layer on top of a 2  $\mu\text{m}$  oxide layer [Fig. 3(d)], with both partial (70 nm) and full (220 nm) etch features

(the general waveguide parameters are similar to those used in Section 2). Three different grid resolutions for defining the grating periods were considered: 2 nm, 4 nm, and 6 nm. As before, vertical grating couplers are used for input and output coupling and to ensure operation with TE-polarized light. Moreover, an on-chip  $1 \times 2$  splitter (Y-branch) allows for extraction of the reflected signal; a schematic of the device is shown in Fig. 4.

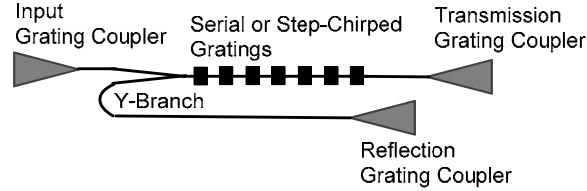


Fig. 4. Schematic diagram and layout of devices.

### 3.1 Serial sidewall Bragg grating arrays

For the serial array, we consider five uniform gratings. We use a starting grating period of  $\Lambda_1 = 336$  nm or 338 nm; the grating periods then decrease in steps of 4 nm in one design and in steps of 6 nm in the other (i.e., using grid resolutions of 4 nm and 6 nm). In both cases, the gratings have a width  $W_1 = 500$  nm, sidewall corrugation depth  $\Delta W = (W_1 - W_2)/2 = 20$  nm, and comprise 2000 periods; the grating duty cycle is 50%. The gratings are separated by a length  $\Delta L = 370$   $\mu\text{m}$  such that the center-to-center spacing between gratings is  $\sim 1$  mm.

Figure 5(a) shows the measured transmission and reflection spectra for the serial grating array with a grid resolution of 4 nm. The individual reflection responses of the gratings overlap slightly to create a quasi-continuous reflection spectrum spanning a range from 1525 nm to at least 1570 nm (spectral measurements were constrained to a wavelength range of 1500 nm - 1570 nm due to limitations of the instruments/experimental setup available). The time delay response is characterized by modulating the output from a tunable laser tuned to wavelengths within each grating band (indicated by the arrows in the spectral response) with a 10 GHz sinusoid and detecting the corresponding reflected signal on an optical sampling module (7.6 ps impulse response) connected to a digital oscilloscope. The operating bandwidth of the C-band EDFA used to compensate for coupling and on-chip losses (between 20 and 30 dB) further limits the wavelength range over which the time delay response is measured (these large losses may be reduced with improved coupling and vertical grating coupler designs). In particular, we can only address 4 of the 5 gratings in the array. We obtain a delay of 60 ps in steps on average of 20 ps. A total delay of 80 ps is expected if we can make use of the grating at  $\sim 1570$  nm in the time delay measurement.

For the array with a grid resolution of 6 nm, 4 separate reflection bands are clearly visible within the wavelength range of the measurement. In this case, the reflection bandwidth spans at least 62 nm. The delay between 3 successive reflection bands is measured to be 29 ps; a total delay of about 60 ps would be expected if all bands were accessible. The results are summarized in Fig. 5(b).

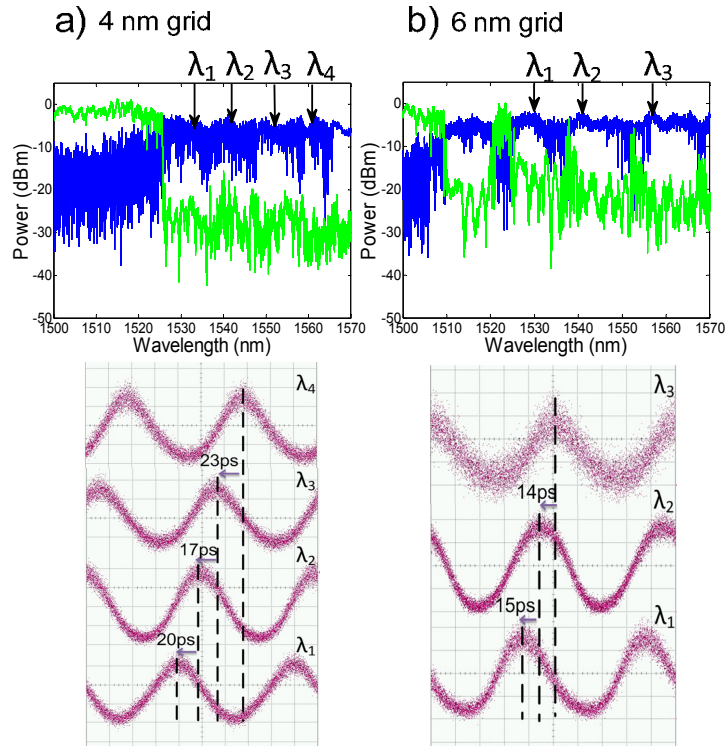


Fig. 5. Serial sidewall Bragg grating arrays fabricated with (a) 4 nm and (b) 6 nm grid resolution. The arrows indicate the wavelengths that are used to measure the delay response (sample mode, persistence time of 300 ms, 20 ps/div). For the spectral measurements, the reflection curves are in blue and the transmission curves are in green.

### 3.2 Step-chirped sidewall Bragg gratings

We consider various step-chirped grating designs based on a fixed corrugation depth of  $\Delta W = 20$  nm and involving different waveguide widths  $W_l$ . In these designs, the overall grating length is set to be  $\sim 2.8$  mm; the grid resolution chosen then determines the number of periods per grating and segments  $M$ . In all of the designs, the grating periods increase by an amount corresponding to the grid resolution starting from  $\Lambda_1$ . Table 1 summarizes the parameters for 3 of the grating structures.

**Table 1. Parameters of step-chirped sidewall Bragg gratings**

Structure	Grid resolution (nm)	Number of segments, $M$	$W_l$ (nm)	Starting period $\Lambda_1$ (nm)
1	2	6	520	310
2	4	5	580	302
3	6	4	540	304

Figure 6 shows the measured reflection and transmission spectra along with the time delay response for the 3 grating structures. For structure #1, we obtain a quasi-continuous reflection spectrum that spans the wavelength range from 1515 nm to 1548 nm for a corresponding bandwidth of  $\sim 33$  nm. The time delay response was characterized using 3 of the 6 wavelengths and the delay between adjacent bands is 14 ps for a total delay 28 ps. A total delay of up to 70 ps is expected if all of the gratings can be used. For grid resolutions of 4 nm and 6 nm, separate reflection bands can be observed. For structure #3, the delay between adjacent bands is  $\sim 30$  ps; if all 4 reflection bands can be accessed, the total delay is expected

to be ~90 ps. Table 2 summarizes the delay characteristics for the serial grating arrays and step-chirped gratings.

Some distortion of the waveforms can be observed and is attributed in part to the ripples in the amplitude response. The ripples may be reduced using apodization techniques.

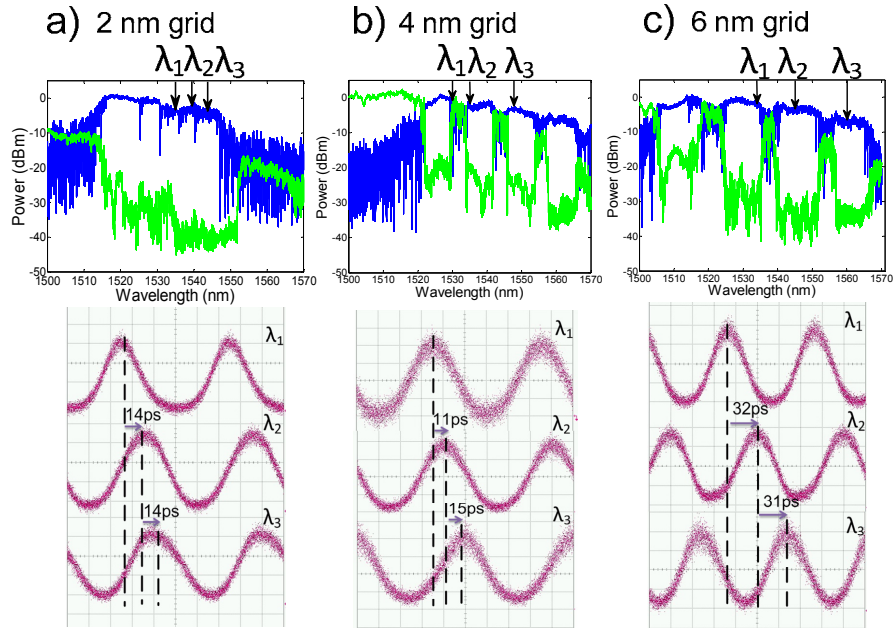


Fig. 6. Step-chirped sidewall Bragg gratings fabricated with (a) 2 nm, (b), 4 nm, and (c) 6 nm grid resolutions. The arrows indicate the wavelengths that are used to measure the delay response (sample mode, persistence time of 300 ms, 20 ps/div). For the spectral measurements, the reflection curves are in blue and the transmission curves are in green.

**Table 2. Summary of delay characteristics for serial grating arrays and step-chirped gratings**

	Grid resolution (nm)	Reflection bandwidth or range (nm)	Average delay between adjacent bands (ps)	Total measured delay (ps)	Total expected delay (ps)
Serial grating array	4	at least 62	20	60	80
	6	at least 45	15	29	60
Step-chirped gratings	2	33	14	28	70
	4	at least 48	15	26	~60
	6	62	31	63	~90

### 3.3 Integration of the grating delay lines and SNWs

As discussed in Section 2.1, efficient and broadband FWM can be obtained in SNWs without a top oxide cladding with a width  $W < 690$  nm. The sidewall gratings were designed with waveguide widths  $W_j$  ranging from 500 nm to 580 nm. As such, the designs of the gratings are compatible with those of the SNWs and both building blocks can be integrated on the same platform (the width of the SNW can be tailored to match the waveguide widths of the gratings/ Y-branch). In particular, the device schematic shown in Fig. 4 can be readily adapted to support this: the waveguide length connecting the ‘Reflection Grating Coupler’ to the Y-branch simply needs to be extended to allow for the generation of sufficient power at

the idler wavelengths. The current waveguide length corresponds approximately to the length of the grating structure which ranges from  $\sim 2.8$  mm for the step-chirped designs to  $\sim 5$  mm for the serial array; on the other hand, an SNW length of 12 mm was used in the experiments shown in Section 2 (the waveguide can be looped to ensure a compact layout). Thus, with a slight modification to the schematic shown in Fig. 4, it should be possible to generate taps through FWM in an SNW and delay them using the grating-based delay. Of course, the device will not allow for any control over the amplitudes of the taps; an integrated spectral shaper would need to be incorporated in the design for this purpose.

#### 4. Summary and conclusion

In this paper, we have described several silicon photonic building blocks that lend themselves for the development of integrated MPFs with reconfiguration capabilities. First, we demonstrated efficient FWM in SNWs for increasing the number of taps in MPFs based on FIR filter designs. Using a readily accessible silicon photonic technology platform, we can design SNWs with anomalous dispersion around 1550 nm for high FWM conversion efficiency over a broad range of wavelengths. Starting from  $N/2$  optical sources at the input, up to  $N$  taps can be generated. The power levels of these taps can then be controlled with a microring resonator-based integrated spectral shaper. The SNWs and integrated spectral shaper can then be combined with high bandwidth silicon-based modulators [26]. Finally, various silicon-based optical delay line technologies are available. To provide tens of ps of delay operating over several to tens of nm of bandwidth, serial sidewall grating arrays or step chirped sidewall gratings can be used. For smaller tap spacings, continuously chirped gratings and tunable gratings are also available. As such, most of the various component technologies to realize an integrated reconfigurable and tunable MPF are readily available (on-chip amplification may be required and in this case, hybrid integration is likely required). Note that the same building blocks can also be exploited to develop an integrated system for generating microwave signals based on FWM in SNW and filtering using Bragg gratings, i.e., fully integrated versions of the subsystems reported in [27,28]. The development of integrated MPFs with reconfigurability and tunability will open the way for a range of cost-effective microwave photonics applications.

#### Acknowledgments

This work was supported by the NSERC NGON CREATE program, the NSERC SiEPIC CREATE program, the Passive Silicon Photonics Workshop, and the FRQNT Programme de recherche pour les enseignants de collège. We thank CMC Microsystems for fabrication assistance, Lumerical Solutions and Mentor Graphics for design software, and R. Bojko at the University of Washington for fabrication. Part of this work was conducted at the University of Washington Microfabrication/Nanotechnology User Facility, a member of the NSF National Nanotechnology Infrastructure Network. We also thank V. Donzella, L. Chrostowski, and N. A. F. Jaeger (University of British Columbia) and D. Deptuck (CMC) for discussions and assistance in device characterization, as well as Z. Saraç and D. Berardo for their contributions.